Communication

Structure-Selective Synthesis of Mesostructured/Mesoporous Silica Nanofibers

Jianfang Wang, Jinping Zhang, Beverly Y. Asoo, and Galen D. Stucky

J. Am. Chem. Soc., **2003**, 125 (46), 13966-13967• DOI: 10.1021/ja036967v • Publication Date (Web): 28 October 2003

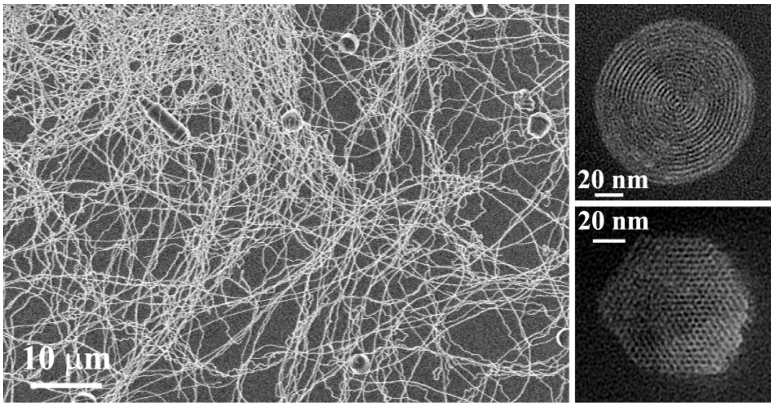

More About This Article

Additional resources and features associated with this article are available within the HTML version:

- Supporting Information
- Links to the 9 articles that cite this article, as of the time of this article download
- Access to high resolution figures
- Links to articles and content related to this article
- Copyright permission to reproduce figures and/or text from this article

View the Full Text HTML

J|A|C|S
COMMUNICATIONS

Published on Web 10/28/2003

Structure-Selective Synthesis of Mesostructured/Mesoporous Silica Nanofibers

Jianfang Wang,[†] Jinping Zhang,[‡] Beverly Y. Asoo,[‡] and Galen D. Stucky*[,†,‡]

Department of Chemistry and Biochemistry and Materials Department, Mitsubishi Chemical Center for Advanced Materials, University of California, Santa Barbara, California 93106-9510

Received June 29, 2003; E-mail: stucky@chem.ucsb.edu

Since the discovery of ordered mesoporous materials,[1] great efforts have been made to modify their morphologies. Acid-catalyzed mesostructure synthesis has proven to be particularly successful in this regard,[2] and the concurrent synthesis and processing of mesostructured fibers,[3,4] spheres,[5] and tubules[6] on the microscopic to macroscopic scale has been demonstrated. Mesoporous materials with designed nanoscopic pores and nanometer-to-larger-scale morphologies are an important new class of materials with enormous potential in sieving, catalysis, and nanofluidics.

An important issue in the applications of nanoscopic mesoporous materials is pore orientation. For example, if the pores in nanoscale mesoporous fibers are aligned parallel to the fiber axis, these fibers could function as nanofluidic channels in applications for electrophoresis and biologically sensitive transistors. Moreover, incorporation and alignment of chemical species,[7] such as polymers, into these nanofibers could offer opportunities for studying transport properties of individual or highly aligned polymer chains, providing valuable information for optimizing polymer-based transistors and diodes.

Early approaches to mesoporous silica fibers employed mechanical drawing[3] and two-phase reactions.[4] Mechanically drawn fibers have diameters of 30−100 μm and consist of multiple ordered domains. The fibers grown from two-phase reactions have diameters from 1 to 40 μm, with a single-crystal-like mesostructure. These fibers were originally believed to have pore channels oriented parallel to the fiber axis,[4a,b] but further investigations showed that the pore channels run circularly around the fiber axis.[4c−e]

Here, we report a simple one-phase route to mesostructured fibers with diameters ranging from 50 to 300 nm and lengths up to millimeters. They are single-crystal-like with hexagonally organized pores and possess either a circular architecture with pore channels running around the fiber axis or a longitudinal architecture with pore channels oriented parallel to the fiber axis. Significantly, we have demonstrated that the internal architecture of these nanofibers can be readily controlled via the synthesis.

Nanofibers with the circular architecture can readily be made using a one-phase route. In a typical synthesis, the silica precursor, tetraethyl orthosilicate (TEOS), was added into a cetyltrimethylammonium chloride (C16TMACl) aqueous solution under a strong acidic condition at room temperature, with the molar ratio of 100H_2O:7HCl:0.02C16TMACl:0.03TEOS. The mixture was then covered and moved into an isothermal oven set at 80 °C, where it was kept without stirring for 1−4 days. Spontaneous growth of suspended flocculates and precipitated particles was observed. The flocculates were taken out, washed with water, and then dried in air. 20−30 wt % of the overall product from each synthesis are flocculates. Scanning electron microscopy (SEM) images show that greater than 90 wt % of the flocculates consist of fibers of lengths ranging from tens of micrometers to several millimeters (Figure 1a). The remaining 10 wt % or less of the content are particles in nature. Examination of individual fibers using transmission electron microscopy (TEM) indicates that the fibers are smooth with uniform diameters along the axis direction and that their diameters range from 50 to 300 nm (Figure 1a, inset).

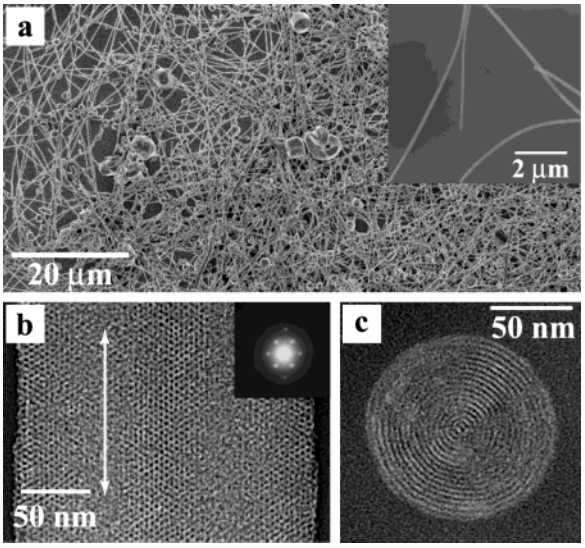

Figure 1. Mesostructured nanofibers with the circular pore architecture. (a) SEM image. The inset is a TEM image. (b) High-magnification TEM image of a 214-nm-diameter nanofiber. The double-arrowed line indicates the fiber axis direction. The inset is a representative electron diffraction pattern. Measurement of the hexagonal lattice constant gives a value of 4.7 nm, in agreement with that determined from XRD. (c) TEM image taken on microtomed nanofiber samples. The diameter of the nanofiber is 113 nm. The measured inter-ring spacing is 3.3 nm, smaller than the value of 4.1 nm determined from XRD, which might be due to compressive strain induced by solidified resin for microtoming.

X-ray diffraction (XRD) patterns reveal a hexagonal mesostructure possessed by the nanofiber sample shown in Figure 1 (Supporting Information, Figure S1). Because XRD only probes the average structure of bulk nanofiber samples, TEM imaging was carried out to investigate the internal architecture of individual nanofibers and their relation to the fiber shape. With the viewing direction perpendicular to the fiber axis, a hexagonally packed array of pore channels oriented perpendicular to the fiber axis was observed over the whole fiber length (Figure 1b). A representative electron diffraction pattern (Figure 1b, inset) further confirms the hexagonal packing of pore channels. To view the pore channel arrangement parallel to the fiber axis, TEM imaging was performed on microtomed thin sections of nanofibers, where the pore channels are visible as concentric rings and the cross section is circular (Figure 1c). Further efforts are needed to determine whether these pore channels are closed-off rings or helices with an extremely small pitch.

It would be intriguing to be able to control the internal arch-

[†] Department of Chemistry and Biochemistry.
[‡] Materials Department.

10.1021/ja036967v CCC: $25.00

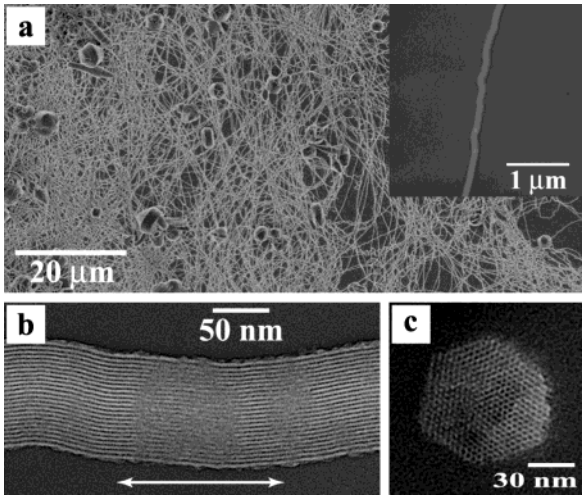

Figure 2. Mesostructured nanofibers with the longitudinal pore architecture. (a) SEM image. The inset is a TEM image. (b) High-magnification TEM image of a 93-nm-diameter nanofiber. The double-arrowed line indicates the fiber axis direction. Measurement of the spacing between parallel pore channels gives a value of 3.9 nm, close to the average value of 4.1 nm determined from XRD. (c) TEM image taken on microtomed nanofiber samples. The spacing between parallel edges of the hexagon is 72 nm. The measured hexagonal lattice constant is 4.1 nm. A value of 4.7 nm was determined from XRD.

itecture of a nanofiber via synthesis. We first tried lowering the growth temperature to 50 °C. High-quality nanofibers were obtained (Figure 2a), and they also have a hexagonal mesostructure, as revealed by XRD patterns (Supporting Information, Figure S1). Individual nanofibers have uniform diameters and slight bends along the fiber axis (Figure 2a, inset), suggesting that these nanofibers might possess a different internal architecture. Indeed, highly organized pore channels parallel to the fiber axis were observed under high-magnification TEM imaging (Figure 2b). Remarkably, TEM images taken on microtomed nanofiber samples indicate that the longitudinal pore channels are also hexagonally packed and that the cross sections of individual nanofibers are hexagonal (Figure 2c). This hexagonal shape results from the minimization of the interior interaction energy among mesostructured domains at the expense of increased external surface energy. The external surface area of the cylindrical fibers is ~95% of that of the hexagonal fibers at a constant cross-section area.

Mesostructured silica nanofibers have been grown under various conditions. The internal architecture of nanofibers can be controlled by varying surfactant, the growth temperature, or by adding inorganic salts.[8] Table 1 summarizes the conditions under which nanofiber samples exhibiting exclusively either a circular or a longitudinal architecture have been obtained (Supporting Information).

N_2 sorption isotherms were measured on calcined nanofibers with C16TMACl as surfactant (Supporting Information, Figure S2). Both types of nanofibers have a BJH pore size of 2.7 nm. Nanofibers with the circular architecture have a pore volume of 0.94 cm^3/g and a BET surface area of 1180 m^2/g, within the range typical for SBA-3 materials.[2] Measurements on precipitated curve-shaped particles[9] grown at either 80 or 50 °C also gave similar values (Supporting Information, Figure S2). By comparison, nanofibers with the longitudinal architecture have a larger pore volume (1.72 cm^3/g) and BET surface area (2050 m^2/g), indicating that some of the pores in the nanofibers with the circular architecture and in the curve-shaped particles are not accessible. This further demonstrates the importance of control of the internal pore architecture of mesoporous materials.

In summary, hexagonally organized mesoporous silica nanofibers have been synthesized. These nanofibers possess either a circular or a longitudinal pore architecture, which can be readily controlled via the synthesis. This structure-selective synthesis could offer opportunities for further understanding the fundamental mechanism governing the cooperative organization of organic and inorganic molecular species into three-dimensionally structured arrays. In addition, the nanofibers with longitudinal pores might find applications in nanofluidic electrophoresis and biochemical sensing.

Table 1. Synthesis Control of the Internal Structures of Nanofibers

architecture	synthesis condition[a]
circular	100H_2O:6.8−7.2HCl:0.01−0.04C16TMACl:0.015−0.06TEOS (80 °C) 100H_2O:7HCl:0.016S:0.022TEOS (S: C16TMABr, C16PCl, or C16PBr, 80 °C)[b]
longitudinal	100H_2O:6.8−7.2HCl:0.01−0.04C16TMACl:0.015−0.06TEOS (50 °C) 100H_2O:7HCl:0.016S:0.022TEOS (S: C16TMABr, C16PCl, or C16PBr, 50 °C) 100H_2O:7HCl:0.003−0.008C18TMABr:0.004−0.02TEOS (80 °C) 100H_2O:7HCl:0.019C16TMACl:0.038TEOS:salt (salt: 0.0001−0.0004NaF, 0.01−0.02NaCl, 0.02−0.2NaBr, 0.01−0.03NaI, 0.01−0.2K_2SO_4, 0.06−0.2Na_2SO_4, or 0.01−0.2KNO_3, 80 °C)

[a] The reaction compositions are given in the molar ratio. [b] C16PCl and C16PBr represent cetylpyridinium chloride and bromide, respectively.

Acknowledgment. We thank M. H. Bartl, J. H. Harreld, and Y. Wu for helpful discussions. This work made use of MRL Central Facilities supported by the National Science Foundation under award No. DMR00-80034.

Note Added after ASAP: The version published on the Web 10/28/2003 contained errors in the caption to Figure 2 and the description of the control of architecture of nanofibers. The Web version published 10/29/2003 and the print version are correct.

Supporting Information Available: XRD patterns, nitrogen sorption isotherms, SEM and TEM images, synthesis conditions, and a brief discussion (PDF). This material is available free of charge via the Internet at http://pubs.acs.org.

References

(1) (a) Yanagisawa, T.; Shimizu, T.; Kuroda, K.; Kato, C. *Bull. Chem. Soc. Jpn.* **1990**, *63*, 988−992. (b) Kresge, C. T.; Leonowicz, M. E.; Roth, W. J.; Vartuli, J. C.; Beck, J. S. *Nature* **1992**, *359*, 710−712.
(2) (a) Huo, Q. S.; Margolese, D. I.; Ciesla, U.; Feng, P. Y.; Gier, T. E.; Sieger, P.; Leon, R.; Petroff, P. M.; Schüth, F.; Stucky, G. D. *Nature* **1994**, *368*, 317−321. (b) Huo, Q. S.; Margolese, D. I.; Ciesla, U.; Demuth, D. G.; Feng, P. Y.; Sieger, P.; Firouzi, A.; Chmelka, B. F.; Schüth, F.; Stucky, G. D. *Chem. Mater.* **1994**, *6*, 1176−1191.
(3) (a) Bruinsma, P. J.; Kim, A. Y.; Liu, J.; Baskaran, S. *Chem. Mater.* **1997**, *9*, 2507−2512. (b) Yang, P. D.; Zhao, D. Y.; Chmelka, B. F.; Stucky, G. D. *Chem. Mater.* **1998**, *10*, 2033−2036.
(4) (a) Schacht, S.; Huo, Q. S.; Voigt-Martin, I. G.; Stucky, G. D.; Schüth, F. *Science* **1996**, *273*, 768−771. (b) Huo, Q. S.; Zhao, D. Y.; Feng, J. L.; Weston, K.; Buratto, S. K.; Stucky, G. D.; Schacht, S.; Schüth, F. *Adv. Mater.* **1997**, *9*, 974−978. (c) Marlow, F.; Spliethoff, B.; Tesche, B.; Zhao, D. Y. *Adv. Mater.* **2000**, *12*, 961−965. (d) Kleitz, F.; Marlow, F.; Stucky, G. D.; Schüth, F. *Chem. Mater.* **2001**, *13*, 3587−3595. (e) Marlow, F.; Leike, I.; Weidenthaler, C.; Lehmann, C. W.; Wilczok, U. *Adv. Mater.* **2001**, *13*, 307−310.
(5) (a) Fowler, C. E.; Khushalani, D.; Mann, S. *Chem. Commun.* **2001**, 2028−2029. (b) Huo, Q. S.; Feng, J. L.; Schüth, F.; Stucky, G. D. *Chem. Mater.* **1997**, *9*, 14−17. (c) Lu, Y. F.; Fan, H. Y.; Stump, A.; Ward, T. L.; Rieker, T.; Brinker, C. J. *Nature* **1999**, *398*, 223−226. (d) Fowler, C. E.; Khushalani, D.; Lebeau, B.; Mann, S. *Adv. Mater.* **2001**, *13*, 649−652.
(6) Lin, H. P.; Mou, C. Y. *Science* **1996**, *273*, 765−768.
(7) (a) Nguyen, T. Q.; Wu, J. J.; Doan, V.; Schwartz, B. J.; Tolbert, S. H. *Science* **2000**, *288*, 652−656. (b) Wu, C. G.; Bein, T. *Science* **1994**, *264*, 1757−1759.
(8) (a) Schmidt-Winkel, P.; Yang, P. D.; Margolese, D. I.; Chmelka, B. F.; Stucky, G. D. *Adv. Mater.* **1999**, *11*, 303−307. (b) Silva, F. H. P.; Pastore, H. O. *Chem. Commun.* **1996**, 833−834. (c) Yu, C. Z.; Tian, B. Z.; Fan, J.; Stucky, G. D.; Zhao, D. Y. *J. Am. Chem. Soc.* **2002**, *124*, 4556−4557.
(9) Yang, H.; Coombs, N.; Ozin, G. A. *Nature* **1997**, *386*, 692−695.

JA036967V